Materials and Design 32 (2011) 1485–1500

Contents lists available at ScienceDirect

Materials and Design

journal homepage: www.elsevier.com/locate/matdes

An investigation into hybrid carbon/glass fiber reinforced epoxy composite automotive drive shaft

M.A. Badie, E. Mahdi *, A.M.S. Hamouda

Mechanical and Industrial Engineering Department, College of Engineering, Qatar University, P.O. Box 2713, Doha, Qatar

ARTICLE INFO

Article history:
Received 8 June 2010
Accepted 25 August 2010
Available online 31 August 2010

Keywords:
Composite
Fatigue
Buckling

ABSTRACT

This paper examines the effect of fiber orientation angles and stacking sequence on the torsional stiffness, natural frequency, buckling strength, fatigue life and failure modes of composite tubes. Finite element analysis (FEA) has been used to predict the fatigue life of composite drive shaft (CDS) using linear dynamic analysis for different stacking sequence. Experimental program on scaled woven fabric composite models was carried out to investigate the torsional stiffness. FEA results showed that the natural frequency increases with decreasing fiber orientation angles. The CDS has a reduction equal to 54.3% of its frequency when the orientation angle of carbon fibers at one layer, among other three glass ones, transformed from 0° to 90°. On the other hand, the critical buckling torque has a peak value at 90° and lowest at a range of 20–40° when the angle of one or two layers in a hybrid or all layers in non-hybrid changed similarly. Experimentally, composite tubes of fiber orientation angles of ±45° experience higher load carrying capacity and higher torsional stiffness. Specimens of carbon/epoxy or glass/epoxy composites with fiber orientation angles of ±45° show catastrophic failure mode. In a hybrid of both materials, [±45°] configuration influenced the failure mode.

1. Introduction

Power transmitted from the engine to the final drive where useful work is applied through a system consists of a gearbox, clutch, drive shaft and a differential in the rear-drive automotives [1]. Different from the conventional metallic, in composite drive shaft there are many parameters to be altered, namely the fibers orientation angles, stacking sequences, layers thicknesses and number of layers [20]. These parameters, due to the tailorability of elastic constants, could provide a large number of possible designs, which must satisfy optimally the performance characteristics of the composite drive shaft (critical speed, critical buckling torque and load carrying capacity). Leslie et al. [2] studied four designs of a drive shaft 50" long and 3" diameter with material consideration of carbon fiber, aluminum, steel and titanium. It is well-known that the steel drive shaft is usually manufactured in two pieces to increase the fundamental bending natural frequency because the bending natural frequency of a shaft is inversely proportional to the square of beam length and proportional to the square root of specific modulus [3]. There are many design studies but the information about the design variables and their effect on the performance characteristics is not comprehensive [4]. It is misunderstood that carbon fiber shafts were "too stiff". Indeed, what meant by too stiff is the torsional stiffness rather than the flexural stiffness. Both the torsional stiffness and flexural stiffness could be tailored due to the type of application. Rastogi [5] used a hybrid of carbon/epoxy and glass/epoxy to optimize the cost versus performance requirements. He analyzed and designed a composite drive shaft using two approaches. The first approach is closed-form analytical expressions for the critical speed, torsional strength and buckling strength, which utilized to develop a preliminary design tool. The effect of fiber orientation angle on the fatigue strength of composite tubes was discussed by many researchers [6–8] but, on the other hand, the effect of stacking sequence on the torsional fatigue strength is not available. Bert and Kim [9] carried out an analytical solution to compute torsional buckling of composite drive shafts. They calculated the torsional buckling load of composite drive shafts with various lay-ups with good accuracy by considering the effect of off-axis stiffness and flexural moment. Their theory can predict the torsional buckling of composite drive shafts under pure torsion and combined torsion and bending. Chen and Peng [10] performed numerical simulation using a finite element method to study the stability of composite shafts under combined loading conditions. They predicted the critical axial load of a thin-walled composite drive shaft under rotation.

Generally, all accessed design studies were not including the fatigue consideration, which may be needed to be explored in relation to composite shafts design. Therefore, the aim of this work is to investigate numerically the effect of stacking sequence and

* Corresponding author. Tel.: +974 4034309.
E-mail address: elsadigms@qu.edu.qa (E. Mahdi).

0261-3069/$ - see front matter © 2010 Elsevier Ltd. All rights reserved.
doi:10.1016/j.matdes.2010.08.042

fiber orientation angle on the performance of drive shaft. The numerical results were validated by results obtained from analytical solutions. Separately, a study of the torsional stiffness, torque–angle of twist behavior and failure modes was experimentally performed in order to enable the observation and discussion of the different failure modes. The specimens used in the experiment were hand lay-up fabricated from woven roving fiber. This fabrication technique is limited to study the behavior of composite tubes rather than to study applicability of this technique to drive shafts.

2. Design factors

2.1. Fundamental natural frequency

Driveshaft is idealized as a simply supported beam. If the exact fundamental deflection (the first mode) assumed, the fundamental frequency found will be the correct one. It is natural because there is no force or damping applied on the structure. When an oscillatory motion repeated in equal intervals of time t, it's reciprocal, $f = 1/t$, is called the frequency. The bending natural frequency in composite tube is:

$$f_n = \frac{\pi}{2}\sqrt{\frac{E_x I}{mL^4}} \tag{1}$$

where m is the mass per unit length. The lateral natural frequency directly related to the lateral stiffness (E_xI) of the drive shaft and since the moment of inertia (I) is only determined by the geometry, then the composite drive shaft can be designed to have higher lateral natural frequency by increasing the modulus E_x.

2.2. Torsional frequency

Another concept is the torsional frequency. This frequency is directly related to the torsional stiffness (T/ϕ), where ϕ, is the angle of twist and T is the applied torque. The frequency of torsional vibration can be presented as:

$$f_t = \frac{1}{2\pi}\sqrt{\frac{K}{I_m}} \tag{2}$$

K, being the torsional spring rate, is equal to the torsional stiffness. I_m is the mass moment of inertia at propeller. For a given geometry of a drive shaft, the torsional stiffness is directly related to the modulus of rigidity (G_{xy}) as follows:

$$K = \frac{T}{\phi} = \frac{G_{xy}J}{L} \tag{3}$$

J, is the polar moment of inertia and L is the length. The shear modulus can be tailored to its maximum value by orienting the fibers at an angle equal to 45°. This shear modulus can be directly obtained from the extensional stiffness matrix [A] by dividing the shear stiffness component A_{66} by the total thickness of the drive shaft as follows:

$$G_{xy} = \frac{A_{66}}{t} \tag{4}$$

The practical application of torsional vibration systems are engines. These engines have damping (source of dissipation of energy) in the crankshafts (hysteresis damping) and in inertias (damping in torsional vibration dampers and in propellers). Since damping present is normally small in magnitude, for determining the natural frequency it is ignored. Fig. 1, which was drawn after the previous reference, presents an illustration of a torsional system of four rotors in a propeller and lateral oscillations with three masses. These illustrations can provide an insight for both the torsional frequency and lateral frequency of driveshaft. Indeed,

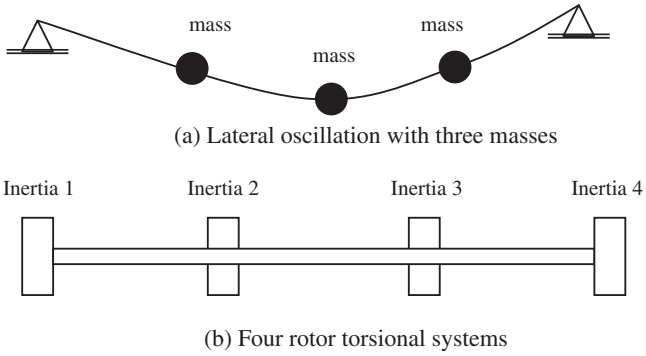

Fig. 1. Illustration of two systems related to lateral and vibration frequency.

the drive shaft tends to bend slightly as it rotates due to the mass imbalance and this bend amplified if the bending natural frequency becomes coincident with the rotational frequency causing the whirling or lateral oscillations of the drive shaft. Then, the bending natural frequency is function of the specific mass (mass per unit length) and the lateral bending stiffness (E_xI). On the other hand, the torsional frequency is related to the mass moment of inertia and the torsional stiffness.

2.3. Critical buckling

An introduction to stress stiffness and buckling concepts, as given by Cook et al. [11] is presented herein: Buckling means loss of the stability of an equilibrium configuration, without fracture or separation of the material or at least prior to it. Bifurcation buckling is the kind of buckling familiar from elementary column theory in which, for an axial compressive load of magnitude P_{cr}, called the critical load, the straight pre-buckling configuration ceases to be a stable state of equilibrium and an alternative buckled configuration is also possible at load P_{cr}. Buckling may also appear without bifurcation. Bifurcation buckling occurs when a member or structure converts membrane strain energy into bending strain energy with no change in externally applied load [8,11]. In slender columns and thin plates or shells, membrane stiffness is much greater than bending stiffness, and large membrane strain energy can be stored with small deformations. When buckling occurs, comparatively large bending deformations are needed to absorb membrane strain energy released. The critical torque can be applied, when [$B_{ij} \approx 0$], is:

$$T_{cr} = 21.75(D_{22})^{5/6}\left[\frac{A_{11}A_{22} - A_{12}^2}{A_{22}}\right]^{3/8}\frac{R^{5/4}}{L^{1/2}} \tag{5}$$

The restriction on this equation is that

$$\left(\frac{D_{22}}{D_{11}}\right)^{5/6}\left(\frac{A_{11}A_{22} - A_{12}^2}{12A_{22}D_{11}}\right)^{1/2}\frac{L^2}{R} \geqslant 500 \tag{6}$$

It is recommended that the T_{cr}, be multiplied by 0.67 for use in design. Another expression to find the critical torque is:

$$T_{cr} = (2\pi r^2 t)(0.272)[E_x E_h^3]^{0.25}(t/r)^{1.5} \tag{7}$$

where t is the overall thickness, r is the mean radius and E_x and E_h are the average moduli in the axial and hoop directions, respectively.

2.4. Design requirements

The drive shaft must be designed to carry the torque without failure. The primary failure mode is fiber failure, and fibers must

be oriented in a way to increase the load carrying capacity. For very thin walled tubes such as composite drive shaft, the possibility of torsional buckling exists. Therefore, design must eliminate any possibility of buckling. The lateral stiffness, which is the product of the axial modulus (E_x) and the moment of inertia (I), must be maximized, because it increases directly the lateral natural frequency. The drive shaft dimensions are selected due to the limited spacing at the automotive. In this design requirement, the length is 1.73 m, and the mean radius is 50.8 mm. The natural frequency must exceed a value of 90 Hz, which describe the rotational frequency. The ultimate torque is 2030 Nm and the ultimate torque for 10^5 cycle reversed fatigue is 678 Nm. This ultimate torque is rather transmitted from a medium duty trucks having an engine of a power higher than 350 hp with this torque measured at low speed of almost 1200 r.p.m. The ultimate strength of both carbon/epoxy and E-glass/epoxy are based on laboratory tests of fatigue after impact. The allowable stress of E-glass–epoxy is the fatigue strength after impact at 10^5 cycles and it equal to 0.25 of the ultimate tensile strength. This allowable value incorporates an allowance for degradation due to fatigue after impact [12]. The low-speed impact and its effect on the fatigue life were discussed extensively [13–15].

2.4.1. Lay-up selection

It is well-known that the shear modulus of many fiber-reinforced composites is lower than that for steel. Thus for an equivalent torsional stiffness, a fiber-reinforced composite tube must have either a larger diameter or a greater thickness than a steel tube [16]. Among the various laminate configurations, $[\pm 45]_S$ laminates possess the highest shear modulus and are the primary laminate type used in purely torsional applications [5]. To meet the minimum resonance frequency, the shaft must have an adequate axial modulus and since the axial modulus of a [±45] laminate is rather low, 0° layer must be added to the lay-up to improve the resonance frequency [3]. The easiest way to increase the critical buckling torque would be to increase D_{22}, which is achieved by adding one or more 90° plies on both sides of the laminate midplane. Therefore, the lay-up selected consists of ±45° glass fiber layers, 0° carbon layer and 90° glass layer at outside surface.

2.4.2. Wall thickness determination

The layers thickness can be found through using different formulas depending upon the density of both fibers and matrix [17]. The minimum wall thickness for the laminate is determined from the following equation:

$$\tau_{all} = \frac{S_{xys}}{n} = \frac{T_{\max}}{2\pi r^2 t} \tag{8}$$

However, the thicknesses selection should be realized after a number of analysis and redesign. In general, the shear modulus of a laminate increases with increasing fiber modulus.

2.4.3. Material selection

Proper selection of the fiber type is very important, since it influences the characteristics of a composite laminate. Accordingly in this study two types of fibers have used. These are E-glass fiber and carbon fiber. E-glass has the lowest cost of all commercially available reinforcing fibers, which is the reason for its widespread use in the FRP industry; therefore two layers are constructed from E-glass fiber/epoxy. On the other hand, the cost factor plays a role in selecting only one layer of carbon/epoxy.

The properties of selected carbon and glass fibers-composite were shown in Table 1. The selected thicknesses for different layers are as follows:

±45° glass/epoxy layers thickness for each = 0.1905 mm; 0° carbon/epoxy layer thickness = 0.635 mm; 90° glass/epoxy layer thickness = 1.016 mm.

3. Finite element analysis

Numerical simulation of a hybrid composite drive shaft is performed using LUSAS version 13.5-7 [18] commercial software. The shaft is assumed to be balanced and the stress–strain relationship is linear and elastic. The method followed to generate a satisfactory model begins with the selection of the element. In this study a three directional thick shell element (QTS8) was selected. The boundary condition was defined and load applied to the model at the directions of local cylindrical coordinates. To evaluate the different effects of layers stacking on the critical performance characteristics and fatigue resistance, eigenvalue analysis was performed in the form of linear buckling analysis to define the critical buckling torque. Modal analysis, which is a technique used with structures dominated by global displacement, was carried out to define the natural frequency of the drive shaft. The fatigue life of the drive shaft was presented in a contour after post-processing linear dynamic analysis. A contour of damage provided by LUSAS is the invert of the fatigue contour, that the quantity of damage at specific zone is inversely proportional to the fatigue life.

3.1. Model development

The composite drive shaft, which is considered as a thin-walled orthotropic tube to predict the buckling load, is also idealized as a pinned–pinned beam to predict the critical speed. Three-dimensional model of the composite drive shaft was developed and typical meshing generated by using three-dimensional thick shell element. This element accounts for varying thickness and enables anisotropic and composite material properties to be defined. This degenerate continuum element is also capable of modeling warped configurations. The element formulation takes account of membrane, shear and flexural deformations. One end of the drive shaft was totally supported and the other was simply supported for buckling analysis, while both ends were simply supported for modal analysis to obtain the natural frequency. The load was applied at cylindrical local coordinate's direction. Typical meshing, loading and support were shown in Fig. 2.

3.2. Element type selection

The element selected for this study is (QTS8), which is a quadratic and quadrilateral, 3D thick shell element. The quadrilateral element uses an assumed strain field to define transverse shear which ensures that the element does not lock when it is thin. The quadratic elements can accommodate generally curved geometry. The nodes for this shell element type will be assigned five global degrees of freedom. Fig. 3 shows this element and Table 2 presents its property. Cylindrical local coordinate dataset has been defined to align the material direction of the composite lay-up,

Table 1
Material properties of E-glass and carbon fibers-composites used in drive shaft.

	E-glass/epoxy	Carbon/epoxy
Volume fraction (%)	60	60
E_{11} (GPa)	40.3	126.9
E_{22} (GPa)	6.21	11.0
G_{12} (GPa)	3.07	6.6
Poisson ratio (υ_{12})	0.2	0.28
Ultimate strength (MPa)	827	1170
Weight density (kg/m^3)	1910	1610

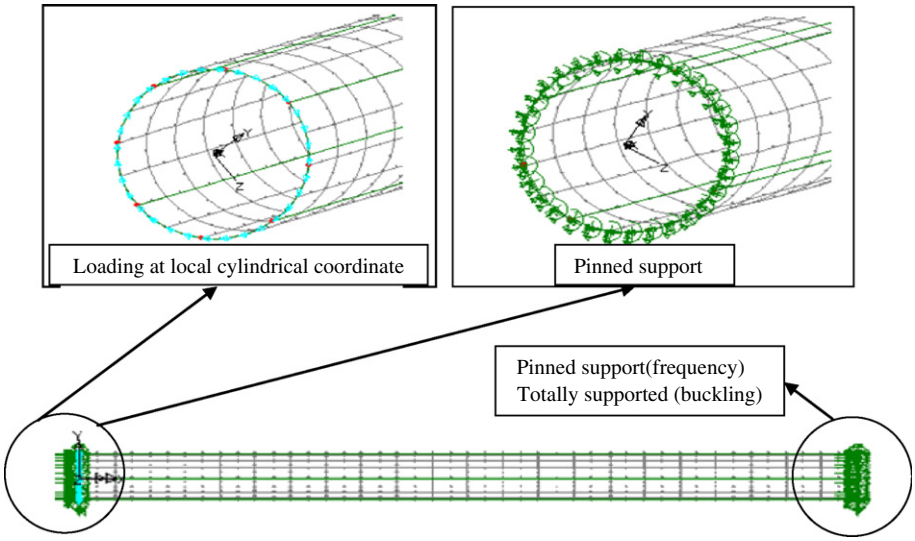

Fig. 2. Typical meshing, loading and support of composite drive shaft model.

support and loading. Internal nodes in a composite mesh are moved to lie on a laminar boundary. Coordinates of a point are specified as (r, θ, z), where (r) is the radius perpendicular to the local z axis; (θ) is the angle in degrees measured from the positive x direction of the local (xz) plane, clockwise about the local z axis when looking in the positive z direction; (z) is the distance along the z axis (Fig. 3). In this system,

$X \equiv r$ (radial direction),
$Y \equiv \theta$ (hoop direction), and
$Z \equiv z$ (longitudinal direction).

In buckling analysis, the model was fully fixed at one end and subjected to torsion load at the other end. In modal analysis which performed to specify the natural frequency, both ends are pinned. Fig. 4 shows the flow chart of numerical and analytical work.

3.3. Types of analysis

Four types of finite element analysis were performed to study the different effects of layers stacking on the critical performance characteristics and fatigue resistance. These are stress analysis, eigenvalue buckling analysis, modal analysis and fatigue analysis.

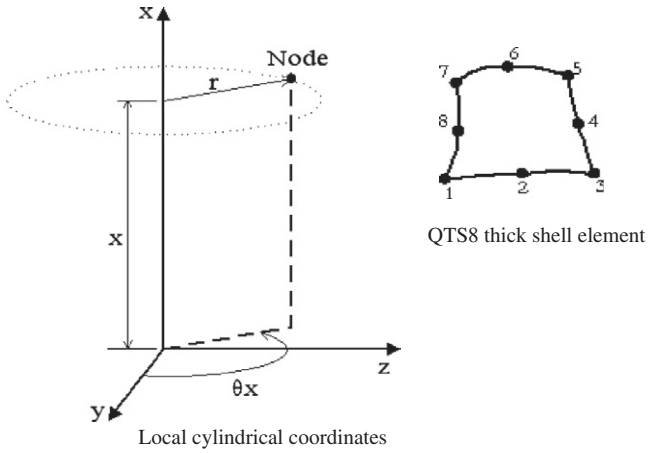

Fig. 3. The (QTS8) element and cylindrical coordinates.

3.4. Stress analysis

The shaft is subjected to torsion at one end and the other end is fixed in axial, radial and hoop direction to perform static analysis. The shear stresses resulting from this analysis used to calculate the torque and the output of the linear eigenvalue analysis is only a factor, which is to be multiplied by the static applied load to obtain the buckling load. The shear stress resultant defined as the through-thickness integral of the planer shear stress or it is also the in-plane force per unit length. The resultant in-plane shear stress can be specified directly from:

$$N_{xy} = \frac{T}{2\pi r^2 t} \tag{9}$$

where r is the radius and t is the thickness. A preliminary composite drive shaft design having formed from a hybrid laminate configuration of [±45/0/90] is chosen throughout this study to be analyzed. The ±45 and 90 fiber orientation plies are of glass/epoxy and 0° ply is of carbon/epoxy.

3.5. Eigenvalue buckling analysis

The objective of an eigenvalue buckling analysis is to obtain the critical buckling load, which is achieved by solving the associated eigenvalue problem. This problem has the same form as a vibration problem, but with mass matrix replaced with stress stiffness matrix. The use of eigenvalue technique to estimate the maximum load that can be supported prior to structural instability is based on the assumptions that the linear stiffness matrix does not change prior to buckling, and that the stress stiffness matrix is simply a multiple of its initial value. The buckling deformation, which represents the mode shape of the structure, is not a quantitative definition of the displacement.

Table 2
The properties of element (QTS8).

Element name	QTS8
Element type	3D thick shell
Group	Shell
Subgroup	Thick shell
Shape	Quadrilateral
Interpolation order	Quadratic

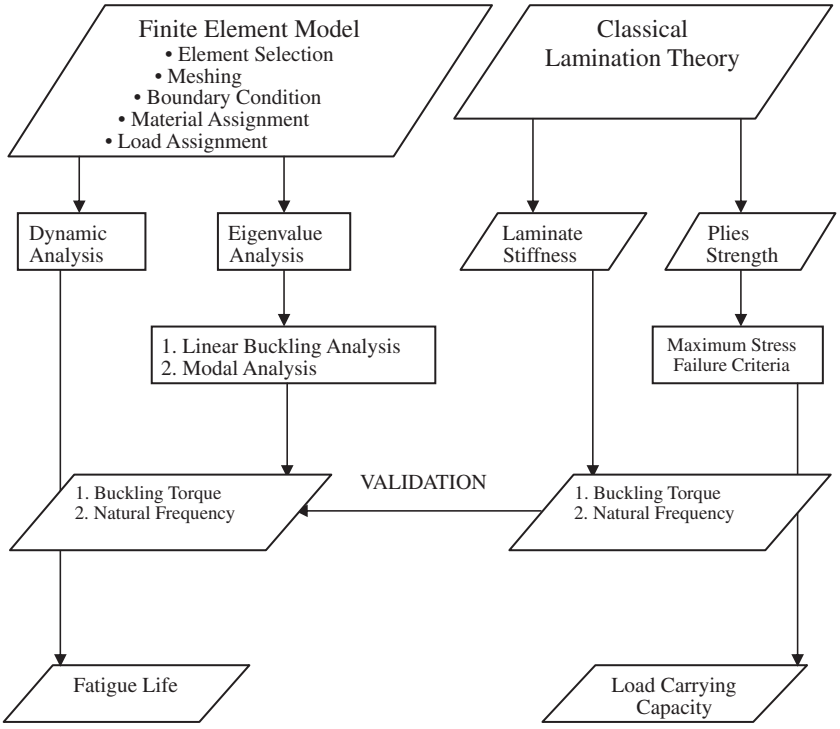

Fig. 4. The flow chart of numerical and analytical work.

3.6. Modal analysis

Modal analysis is a technique used to solve a set of equations to obtain the unknown displacement from each equation. This technique used to find the natural frequencies, because vibration problems are dominated by global displacements affect the whole structure and not like local displacements resulted from impact loads. In impact loading a large number of modes are needed for this wave propagation problem. Reduced set of degrees of freedom are used in modal analysis and then solving for them as function of time to obtain the natural frequencies and modes. In modal analysis dynamic equations are decoupled and there is no need for fine meshing because the stress output is not required. Also there is no need to apply a load because only the natural frequency required. The boundary condition of drive shaft is pinned–pinned and it is simply supported at both ends. As the ends gripping is very considerably affect the natural frequency, the validated support is to make the ends fixed at hoop direction (Y) and free at other degrees of freedom. The lateral natural frequencies are found from modal analysis then multiplied by 60 to obtain the critical speed.

3.7. Fatigue analysis

Based on the results of linear stress analysis, LUSAS provide a post-processing fatigue analysis. The damage done to a structure is used as a measure of how many loading cycles the structure will withstand before failure. Failure occurs when the damage reaches unity (LUSAS user's manual). It was found that, the carbon fibers have better fatigue properties than glass fibers. Also a torque transmission tube of ±45° fiber orientation angle has better fatigue properties than that of 0° angle [19,20]. Comparative S–N diagrams of different layers stacking are investigated after plotting the maximum shear stress versus the logarithm of number of cycles to failure. These values obtained by applying loads of different magnitude to the drive shaft model for every stacking sequence. Then, from the post-processing fatigue analysis the maximum stress calculated and a contour of the corresponding cycles to failure obtained. The S–N curve is used to calculate the number of cycles to failure for each loadcase. Miner's rule is then used to combine the damage for each loadcase to give the total damage to the structure for the specified loading sequence. The damage caused by a single stress magnitude is defined as the ratio of contributing cycles to the cycles to failure, and the total damage is the linear sum of the damages done by individual stress magnitudes. Log values are used because of the large variation in magnitude of the input data. Fatigue calculation of the drive shaft life is defined from the Utilities menu in Lusas using the following menu commands:

3.7.1. S–N curve

Is a curve used to express damage done to a structure for a given number of loading cycles. It contains the assumed variation in log stress/strain values with the number of cycles to failure. The curve is considered linear in the log–log domain. The log stress/strain used to have a range from 4.7323 to 9.7323 after a Lusas example or any adequate range. The log cycle was taken to be from 0 to 15.

3.7.2. Fatigue spectra

Is only available when a linear analysis results file is open and it is a loading spectrum defining the loading sequence in terms of a series of loadcases, each of which has an associated load factor and number of cycles. As we want to plot the number of cycles to failure, then the number of cycles entered in the fatigue spectrum should sum to unity. The factor also should be unity.

3.7.3. Fatigue loadcase

The fatigue results are then configured using a fatigue loadcase, which allows previously defined S–N curves and fatigue spectra to be combined. The results entity specified in this dialog is used to calculate the fatigue life. Once defined fatigue loadcases are contained in the loadcase tree view. From the fatigue loadcase

the selected entity is the stress (S) and the selected component is the shear stress (S_{xy}). The maximum shear stress is defined from the utilities menu using the menu command (print result wizard), then the log of the maximum shear stress calculated and saved. As the plot is linear, then only three results could satisfy plotting the graph. The procedure repeated for different stacking sequences.

4. Close-form analytical work

Classical lamination theory is used in finding and analyzing the design requirements to evaluate the strength, stiffness and stability of the drive shaft structure. The natural frequency, buckling torque and shear strength of one specimen from the six fabricated specimens was obtained by a close-form analysis. This specimen was fabricated from a glass woven fabric composite with fibers oriented at ±45° angle. The results from the analytical solution were used to validate the numerical results obtained from the finite element analysis. In addition, numerical and analytical works were carried out on a full scale hybrid drive shaft.

5. Experimental work

The prospective results of experimental work are aimed to irrecusably investigate the torsional stiffness of the composite drive shaft. The behavior of composite tube under various stacking sequence and fiber orientation angle should be investigated. Carbon and glass woven roving fabrics are used with epoxy to manually fabricate six composite tubes with dimensions scaled down from the designed drive shaft. Four volume units of epoxy (WM-215TA) having a viscosity of 5.5 Pa s at 30 °C, was mixed with one unit of 0.3 viscous hardener (WM-215TB) to conform the matrix. The elastic properties of the glass/epoxy laminate were presented in Table 3.

5.1. Specimens fabrication

Four layers of carbon/epoxy, glass/epoxy and a hybrid of both were wrapped around aluminum tubes of length equal to 216 mm and outside diameter equal to 12.7 mm. For easily removing the aluminum tubes, thin film of oil was formed then a thin plastic sheet wrapped around. The epoxy impregnated carbon and glass fabrics had been wrapped with plastic sheet at outside surface for the purpose of producing smooth surface. These tubes are removed after curing under room temperature. Fig. 5 shows the aluminum tube, plastic sheet and produced specimens. The ends of the specimens were reinforced by the winding of carbon or glass fibers tows used in filament winding. The stacking of these specimens is as follows:

$[45°]_4$ All layers are of glass/epoxy	$[90°]_4$ All layers are of carbon/epoxy
$[45°]_4$ All layers are of carbon/epoxy	$[(45°)_2$ Glass/$(90°)_2$ carbon]
$[90°]_4$ All layers are of glass/epoxy	$[(45°)_2$ Carbon/$(90°)_2$ glass]

Table 3
Elastic properties of glass fabric/epoxy laminate.

Longitudinal Young modulus, E_{11}	12.85 GPa
Transverse Young modulus, E_{22}	10.24 GPa
In-plane shear modulus, G_{12}	1.49 GPa
Major Poisson's ratio, υ_{12}	0.143
Density, ρ	990.1 kg/m^3

Woven roving fabric fibers used in both [0/90] and [±45] lay-up. The thicknesses of the composites were measured to be:

Carbon/epoxy layer thickness = 0.35 mm.
Glass/epoxy layer thickness = 0.37 mm.

5.2. Testing procedure

Torsion test machine (supplied by Norwood Instruments Ltd.) was used to perform the test. The testing machine with a specimen mounted on it, is shown in Fig. 6. The torque was applied manually by a handle at a geared head. This torque is reacted by a transducer and displayed digitally. The angle of twist was measured over a specified gauge length. For the purpose of the specimens gripping, a steal cylinder was used for this reason. This cylinder was longitudinally divided into two parts and these parts were bolted together. The hexagon head of a steel bolt was welded to the lower part of the cylinder and through a spanner socket held onto the machine shaft. The specimens and their grip were both drilled to insert a pin through them for securing the specimens from slipping during the test. Static torque was applied gradually to the specimens until they failed.

5.3. Validation of finite element analysis

The devising of a mathematical model in finite element analysis requires a reliable input data to predict the physical behavior of this model. The data about geometry, element, loads, boundary conditions and material properties is the source of uncertainty in the FEA results validity. In this study, two preliminary analysis based on analytical close-form work was performed to validate the FEA results. The analysis of one of the specimens used in the experimental work and a full-scale drive shaft was carried out. The two cases used for the validation are:

1. *Analysis of the specimen:* A specimen fabricated from glass woven fabric and epoxy with stacking of $[\pm45]_4$ was used to validate the subsequent finite element results.
2. *Analysis of a full-scale drive shaft:* An analytical solution of both the natural frequency and buckling torque were uses to validate the numerical solutions obtained from a finite element analysis. The buckling torque of the specimen is 59.12 Nm as obtained from the analytical solution and 54.22 from the numerical analysis. The bending natural frequency of the specimen is

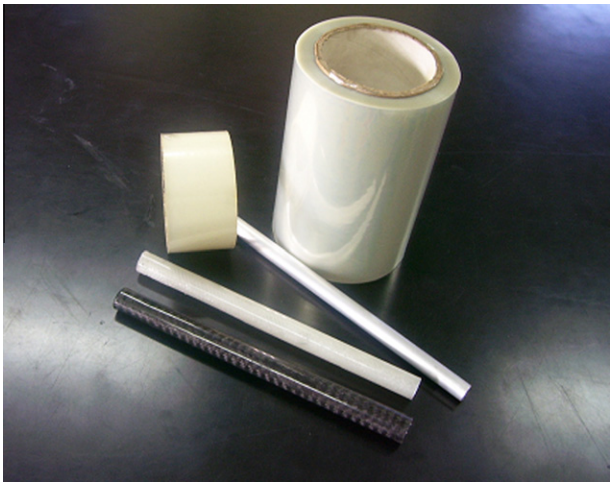

Fig. 5. The aluminum tube and plastic sheets used to produce the shown specimens.

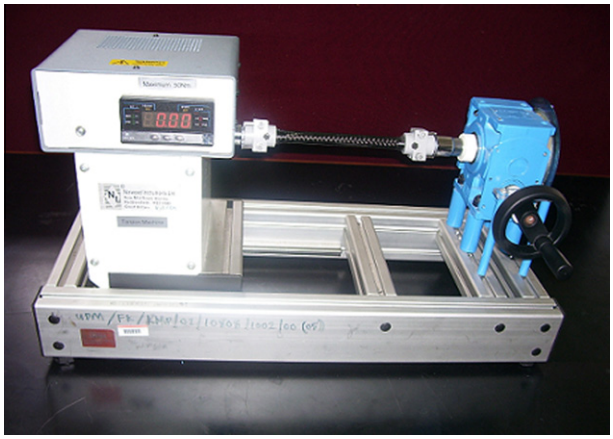

Fig. 6. Torsion test machine with a specimen mounted on it.

375.27 Hz not much differs from the value obtained from the FEA and equal to 377.33 Hz. For the full-scale drive shaft model, the buckling torque from the close-form solution is 2030 Nm and from FEA is 1830.9 Nm. The natural frequency is 91.169 Hz analytically, and 90.46 Hz numerically obtained. Indeed, experiments were needed to be carried out on a full-scale drive shaft to investigate the real buckling torque.

6. Results and discussion

In this section, both finite element analysis and experimental results were presented. The design example is used for the validation of the results obtained from finite element analysis utilized to study the mechanical behavior of composite drive shaft. The experiments oriented only to study the torsional stiffness with its relation to the type of material, fibers orientation angle and stacking sequence. Studying failure modes were another intension of experimental work.

6.1. Finite element results

Finite element models developed to investigate the effects of fibers orientation angles and stacking sequence on the critical mechanical characteristics of the composite power transmission tubing. The critical buckling torque and critical natural frequency estimated by performing eigenvalue analysis. Linear dynamic analysis conducted to study the fatigue responses.

6.1.1. Effect of fiber orientation angle on natural frequency

As the vibration problem has a set of equations, there is a natural vibration mode for every equation that can be extracted by using an eigenvalue extraction analysis. The displacement behavior dominating any structure under vibration is global, therefore modal analysis technique utilized in this type of problems. In modal analysis, the model of the drive shaft does not need a fine meshing because the stress output is not required. Also there is no need to apply a load because the natural frequency is only function of mass and stiffness. The ends of the drive shaft model are both simply supported and the boundary condition must be varied until in specific condition the value of the natural frequency become almost coincident with that presented by a reliable solved example. This checking procedure attributed to the unspecified gripping condition of the orthotropic thin tube from which the idealization of the drive shaft generated. It was recognized that, the ends supports must be applied to the edges of the drive shaft and the circumferential freedom required to be constrained. It is evident that, the contact area between the shaft tube and the yoke joint in addition to the type of joining were not considered in the calculations of the natural frequency. In any structural design having the vibration consideration, only the first mode is of concern for engineering applications. Fig. 7 presents the first mode shape of bending natural frequency. On the other hand, some locally affected structures like that affected by high-energy impact loading need to have all the frequency for the purpose of studying the wave propagation. Fig. 8 shows a set of the first 6 bending natural frequencies ad their mode shapes. The drive shaft of the material and geometry specified was used to investigate the effect of fiber orientation angle on the natural frequency. This structure consists of four layers stacked as $\left[+45^{\circ}_{glass}/-45^{\circ}_{glass}/0^{\circ}_{carbon}/90^{\circ}_{glass}\right]$. From Figs. 9 and 10 it is clear that, the fibers must be oriented at 0° to increase the natural frequency by increasing the modulus of elasticity in the longitudinal direction of the shaft. This explains why the carbon fibers, with their high modulus saved to be oriented at zero angle. In Fig. 9, despite the configuration [0, 0, 90, 0] results in the highest natural frequency, it is not selecting when optimization with another characteristics like the buckling and fatigue strength. From Fig. 10 the drive shaft loses 44.5% of its natural frequency when the carbon fibers oriented in the hoop direction at 90° instead of 0°. The analysis conducted on comparatively thin composite tubes, shows that the behavior of the thinner tube is different and the critical speed or the natural frequency not increases regularly as the orientation angle approaches the value of zero. From Fig. 10, three models of the same material (carbon/epoxy) and different thicknesses were constructed. It is found that the critical speeds for all models are the same when the fibers of all layers oriented at 38–90°. The angle 38° or 37° has unique consideration since at this angle, the unidirectional off-axis tubes under pure torque loading, exhibit the maximum coupling between shear

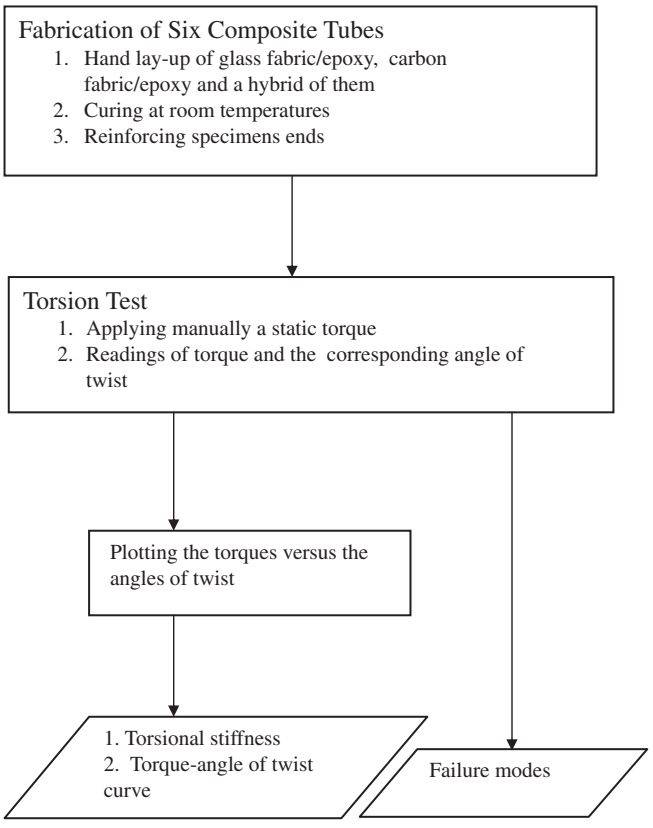

Fig. 7. The flow chart of the experimental work.

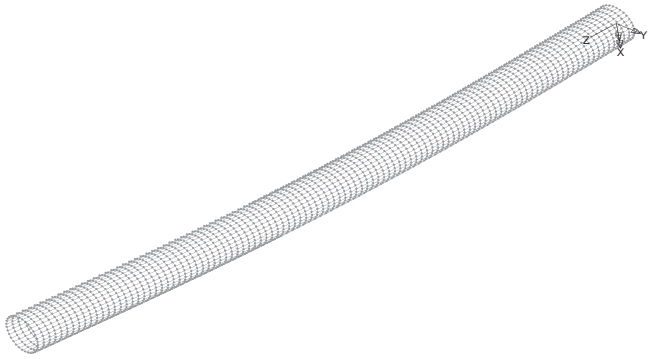

Fig. 8. The first mode of natural frequency.

strain and axial strain. The axial strain reaches to as much as 50% of the shear strain. However, from Fig. 10, it is clear that at the tubes of smaller thickness, the membrane stress plays an effective role in the lateral stiffness of the tube. At 38°, the torque coupling coefficient ($\xi_{T\varepsilon}$) is the maximum and hence the axial strain is the maximum. This directly leads to the highest bending stiffness, which means a higher natural frequency. The stacking sequence has no effect on the natural frequency, because the matrix form of the equation of dynamic equilibrium of elastic body only contain stiffness and mass matrices when no damping and external forces applied. The mass matrix is function of the total density and only the absence of loads make the stacking sequence of no effect. This finding is supported by the fact the boundary conditions of the shaft do not have much effect on the buckling torque. The latter is significantly affecting the vibration mode and by increasing the applied torque, the lower modes of vibration are replaced by the higher ones.

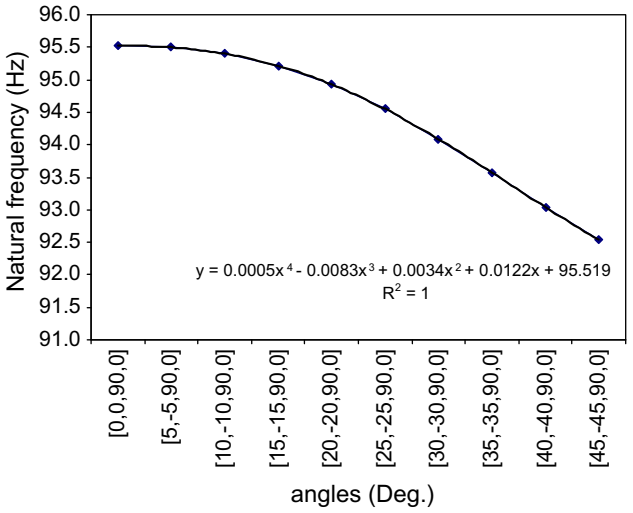

Fig. 10. The effect of fiber orientation angle on the natural frequency by changing the first two ±45 layers.

6.1.2. Effect of fiber orientation angle on buckling torque

A linear eigenvalue buckling analysis conducted to estimate the maximum torque that can be supported prior to losing stability. In this analysis, the specified load must be closer to the collapse load in order to obtain accurate results. The output from the analysis is a factor and this factor multiplied by the actual magnitude of the applied load to obtain the critical torque. Fig. 11 presents the contour of maximum shear stress and the deformed shape after linear Eigen analysis. From the contour of maximum shear stress, it could be observed that higher shear stress accumulated at two bands

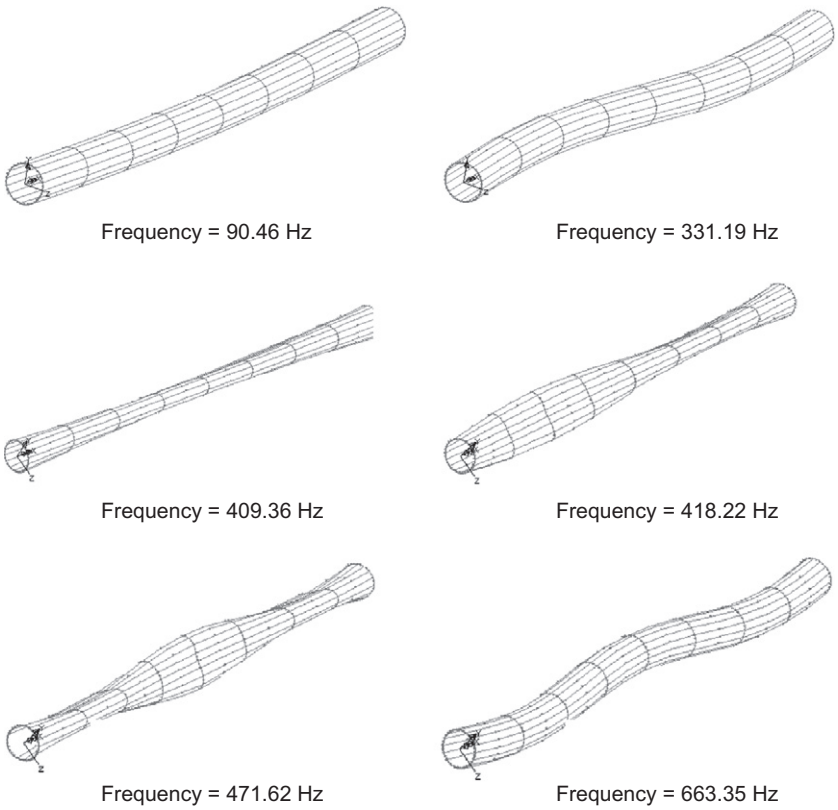

Fig. 9. Set of the first six mode shapes of natural frequency and the corresponding frequency values.

helically wrapping the cylindrical tube at 45° angle. The tubes are buckled when they lose their stability and the circular cross-sections become oval ones. Since the Finite Element model have no imperfection or any defect to specify the two facing location of the cross-section at which the diameter tends to reduce, the accumulation of shear stress in a band forms explains the locations where the buckling occurs or the location at the cross-section that more susceptible to deflection due to a reduced bending stiffness along the hoop direction.

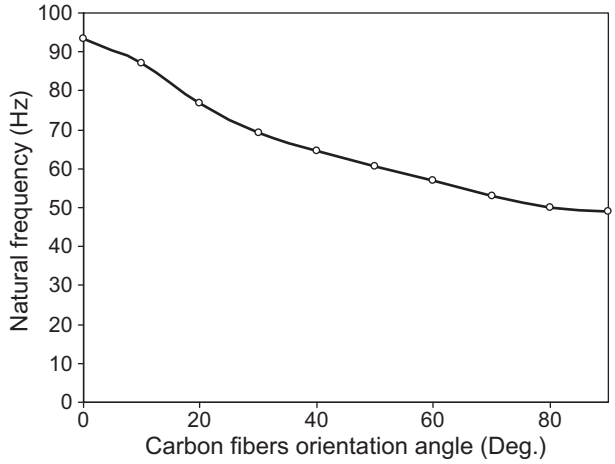

Fig. 11. The effect of changing the carbon fibers orientation angle in a hybrid drive shaft of stacking $[+45^{\circ}_{glass}/-45^{\circ}_{glass}/0^{\circ}_{carbon}/90^{\circ}_{glass}]$ on the natural frequency.

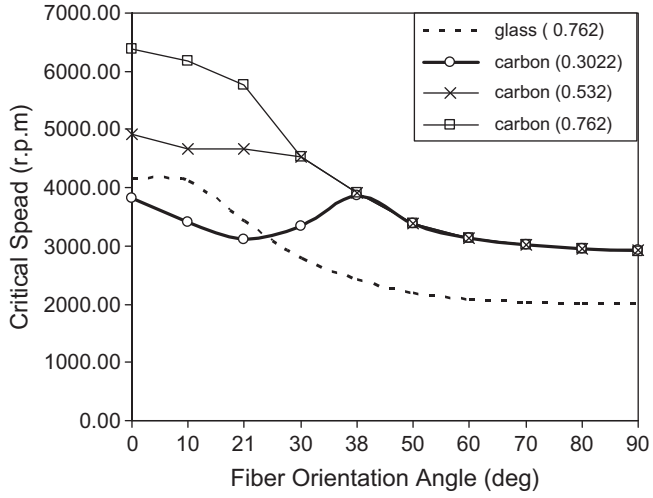

Fig. 12. Comparisons between the critical speeds of composite tubes having four layers and stacking of $[\theta]_4$. *Note*: 1 – glass and carbon are abbreviation of glass/epoxy and carbon/epoxy 2 – figures in parentheses indicate total thickness in millimeters.

The best fiber orientation angle for maximum buckling strength is 90°. At this angle the fibers oriented in the hoop direction and therefore the modulus (E_h) increased. Fig. 12 presents the effect of changing the fiber orientation angles of only two glass/epoxy layers on the buckling torque. As shown in Fig. 13 the behavior of the graphs is not the same in changing the angles of different layers and it is clear that, when changing the angles of the 3rd or the 4th layer or both of them, the critical buckling torque of the drive shaft is not regularly affected by the fiber orientation angles. This attributed to that, the modulus E_x has its maximum value at 0° fiber orientation angle and the modulus E_h has its maximum value at 90° angle. Since the expression of buckling torque if related to both moduli, then the peak value for this torque realized when the fibers oriented at 0° and 90°.

6.1.3. Effect of layers stacking sequence on buckling torque

It is proven that the static torque capacity of drive shaft is significantly affected by changing the winding angle, stacking

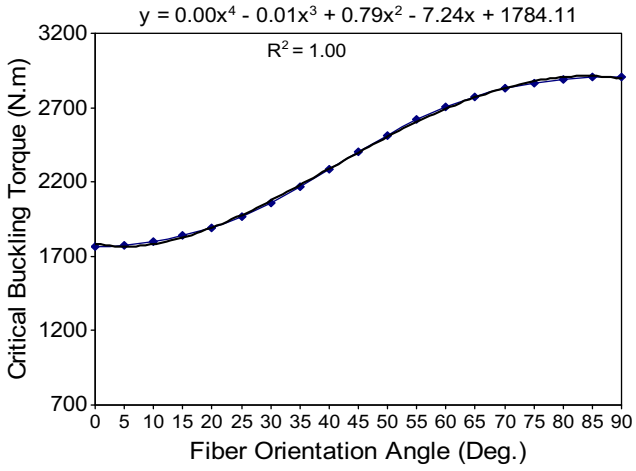

Fig. 14. Effect of fiber orientation angle on buckling torque by changing the first two layers of stacking $[\pm\theta^{\circ}_{glass}/0^{\circ}_{carbon}/90^{\circ}_{glass}]$.

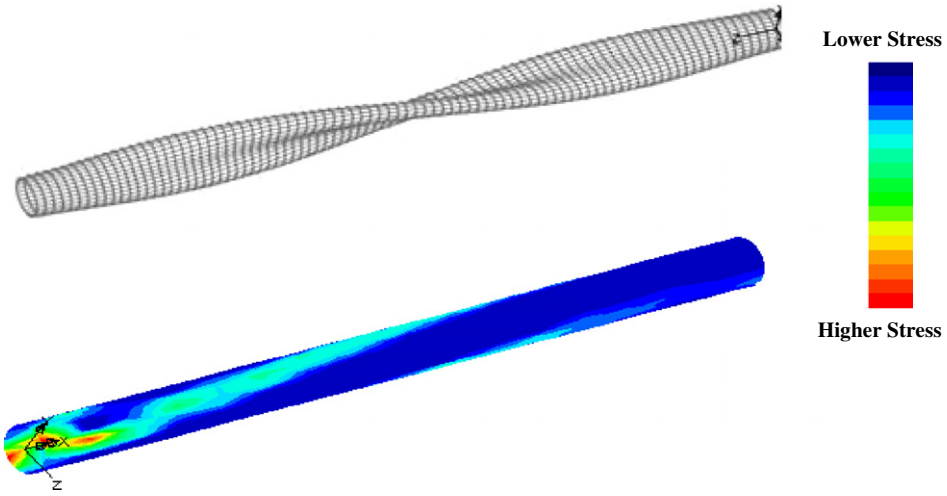

Fig. 13. First mode shape of buckling and corresponding contour of maximum shear stress.

sequences and number of layers. As the [A] matrix is independent of the stacking sequence, both [B] and [D] matrices are dependent. The drive shaft buckled when its bending stiffness along the hoop direction cannot support the applied torsion load. This normal bending stiffness is correspondent to the component D_{22} of the bending stiffness matrix [D]. Therefore, the value of D_{22} specify the buckling strength. Fig. 14 presents the effect of stacking sequence on the buckling strength and it is concluded that the best stacking sequence is [45/−45/0/90] and the worst is [0/90/−45/45]. Table 4 shows the correspondent D_{22} components for selected five laminates with different layers stacking sequences. The best stacking offers a buckling torque of 2303.1 Nm and the worst stacking offers a torque of 1242 with a loss in buckling resistance capability equal to 46.07%. Similar results obtained by Mahmood et al. [6]. They observed that the ply sequence has an important effect on the torsional buckling of the drive shaft. In similar manner, the fiber orientation angle increases, the torsional buckling load increases.

Table 4
Five selected laminates with different stacking sequences and their corresponding stiffness component D_{22}.

Layers stacking sequence	D_{22} (Pa m^3)
[45, −45, 0, 90]	58.8
[0, 45, −45, 90]	55.4
[0, 45, 90, −45]	42.9
[45, −45, 90, 0]	36.31
[0, 90, −45, 45]	36.23

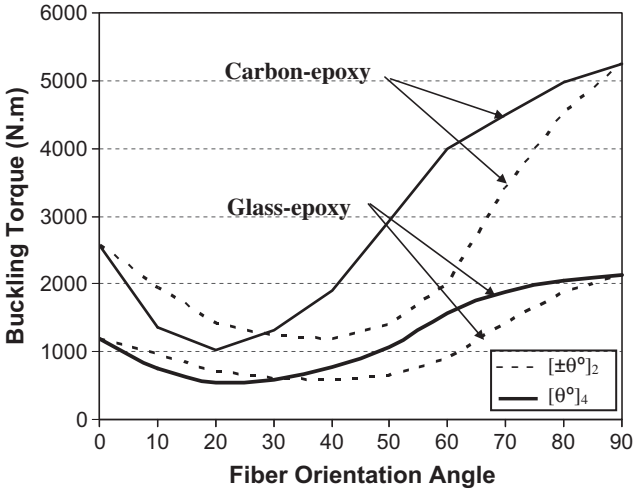

Fig. 15. The effect of coupling between twist moment and normal curvature at hoop direction on the buckling torque.

6.1.4. Effect of coupling between twist moment and normal curvature

The twist moment resulted from a pure torque loading, coupled with a normal curvature in terms of the components D_{16} and D_{26} of the bending stiffness matrix [D]. The D_{16} component represents the curvature at the longitudinal direction and as its value increases, the drive shaft tends to bend and it's bending natural frequency decreases. The coupling between the twist moment and the normal curvature at the hoop direction could be directly related to the coefficient of mutual influence (η), which is a normal-shear coupling.

One kind of this coupling is as:

$$\eta_{x,xy} = \frac{\varepsilon_y}{\gamma_{xy}} = \frac{\bar{S}_{26}}{\bar{S}_{66}} \tag{10}$$

This coefficient represents the radial strain resulted from a torque loading and it may has a negative or positive value. Then, if the sign is positive, the diameter of the cross-section tends to decrease or the curvature at the hoop direction (D_{26}) tends to increase. In angle-ply laminates that consist of 0° and 90° angles do not

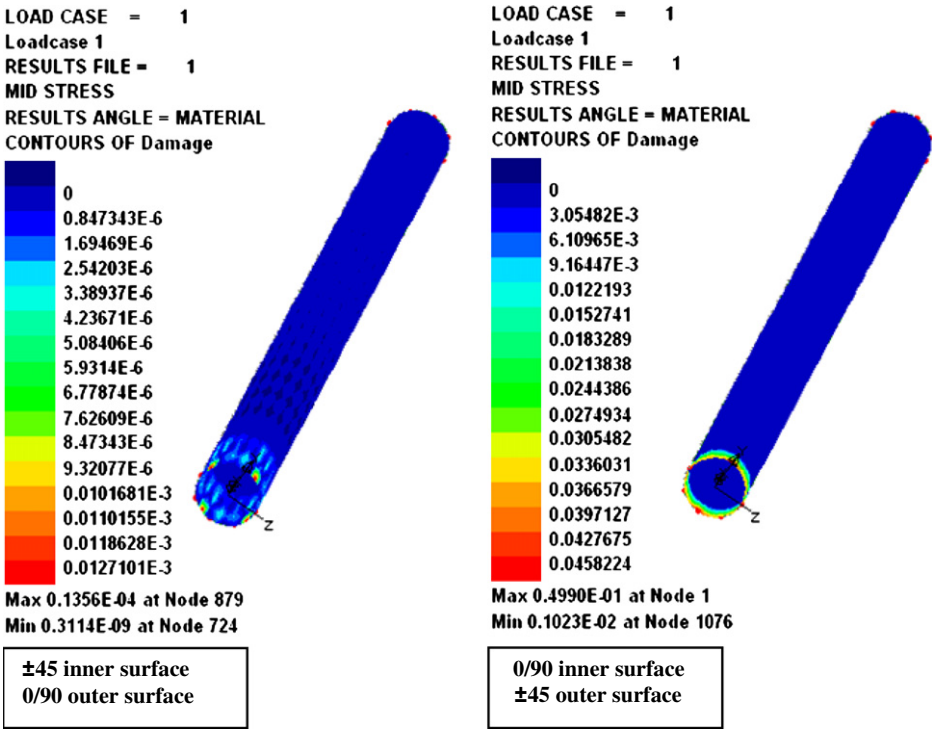

Fig. 16. Comparison between damage tolerance of two configurations of a carbon/epoxy drive shaft with different locations of plies ±45 and 0/90.

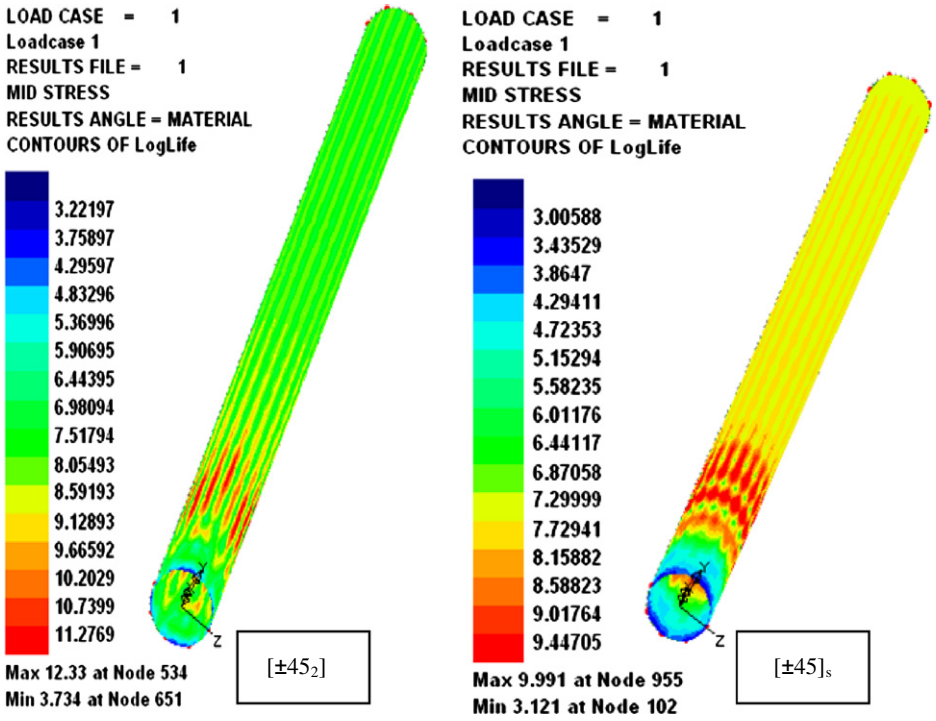

Fig. 17. Contour of loglife of carbon fiber/epoxy drive shaft at symmetrical and unsymmetrical configurations.

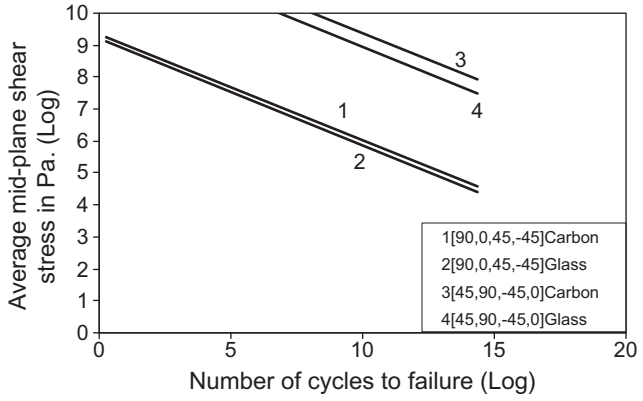

Fig. 18. Effect of stacking sequence on fatigue resistance with comparison between two configurations utilizing all carbon/epoxy or all glass/epoxy layers.

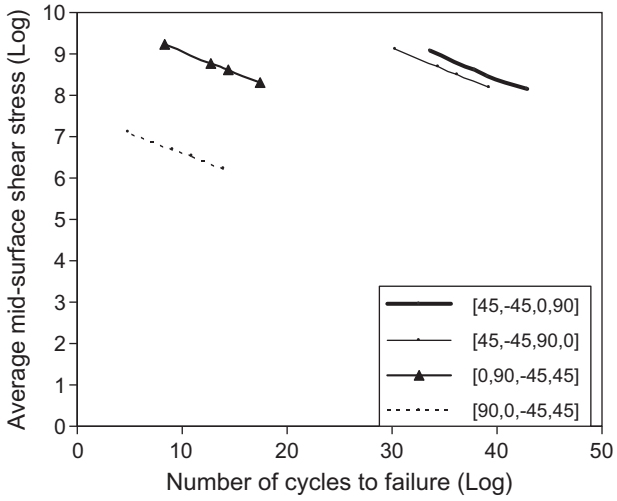

Fig. 19. Torsional S–N diagrams for selected different stacking sequence configurations.

experience such coupling. On the other hand, a configuration of $[\pm\theta_{2n}]$ has a zero coupling or zero D_{16} and D_{26}, because for every $+\theta$ there is $-\theta$ at the same distance from the mid-plane, but the laminate of the configuration $[\theta_n]_S$ has a coupling. Then the component D_{26} and its sign contribute to affect the buckling strength of the drive shaft. Fig. 15 shows the effect of coupling on the buckling torque for two configurations having the same value of the component of normal bending stiffness at the hoop direction D_{22}. However, the difference in the coefficients of mutual influence coupling between twist moment and normal curvature would create divergent shear strains in various laminas only if they were not bonded. For a bonded laminate as the case of this study, equal shear strains for all laminas require the development of interlaminar shear stress τ_{zx}. Although the force equilibrium in the y direction is maintained by the action of σ_{yy} and τ_{yz}, the force resultants associated with σ_{yy} and τ_{yz} are not collinear. The moment equilibrium about the x axis is satisfied by the action of the interlaminar normal stress σ_{zz}.

6.1.5. Fatigue strength

It is known from previous studies that the torsional fatigue exhibit linear behavior on the S–N plot scaled as log–log. The torsional fatigue strength of ±45° carbon/epoxy specimen is approximately 3.7–3.8 times higher than that of the 0° specimens at an equivalent number of cycles. Khalid et al. [2] studied the bending fatigue of composite overwrapped aluminum tube. They used filament winding process to fabricate the articles. They used glass fiber/epoxy to design the overwrapped composite. Four cases were studied using aluminum tube wounded by different layers of composite materials and different stacking sequence or fiber orientation angles. Their results indicated that the cracks initiating in the zones free of fibers or in the outer skin of resin and increase

with increasing number of cycles until the failure of specimen. In this study the effect of layers stacking sequence has been investigated. It is found that, the stacking sequence has no effect on the fatigue life when the maximum stress at the axial direction is considered to obtain the number of cycles to failure. When the maximum shear stress used to plot the S–N diagram, the stacking sequence also has no effect. Only the average mid-surface plane shear stress is the stress that gives different fatigue cycles to failure for different stacking sequence. The worst zone of the drive shaft from fatigue resistance side of view is the gripping zone. From Fig. 16, the amount of fatigue damage that the drive shaft sustains has its maximum values at the gripping zones but the damage tolerance for the all drive shaft structure is much better when the layers having fibers oriented at ±45° located at the inner face of the tube, while locating the layers of fibers oriented at 0/90 at inner face provides less damage tolerance of any composite torque tube. Fig. 17 presents the contours of loglife of two drive shafts having laminates configurations of $[\pm 45_2]$ and $[\pm 45]_S$. From this figure, the effect of coupling between the twist moment and normal curvature at hoop direction, is seem to play another role in terms of the fatigue life of the drive shaft and it clear that, there is a relation between the buckling strength and the fatigue strength. As mentioned earlier, the drive shaft of symmetric configuration laminate experiences less fatigue life due to the existence of the coupling terms D_{16} and D_{26} if compared with the asymmetric configuration. On the other hand, and as mentioned before, changing the sign of this configuration as $[-45/+45]_S$ instead of $[+45/-45]_S$ will increase the fatigue life to be more than the configuration $[\pm 45_2]$. As the fatigue resistance for any structure can be evaluated in the S–N diagram by the inclination and location of plotted lines compared to each others. The less inclination and top position is the best. Fig. 18 shows a comparison between two configurations having the same physical geometry but different stacking sequences. Each configuration has the two cases of all its layers are of carbon/epoxy or all of glass/epoxy. From this diagram, the evidence of higher effect of stacking sequence over the effect of material type is clear. Fig. 19 presents comparison between S–N diagrams of different stacking sequences for layers of the same thicknesses, materials and fiber orientation angle. It can be concluded that, in designing for fatigue consideration, the layers of ±45° fiber orientation must kept close to each other and have a location near to inner surface not to be exposed at outer surface. For buckling strength, location of the ±45° layers near to the inner or outer surfaces, as in [45, −45, 0, 90] and [90, 0, −45, 45] configurations, has no effect since their hoop normal stiffness term D_{22}

Table 5
Comparisons between fatigue and buckling strengths for different stacking configurations of $[\pm 45^\circ_{glass}/0^\circ_{carbon}/90^\circ_{glass}]$.

Configuration	Ranking due to fatigue strength	Ranking due to buckling strength
[45, −45, 0, 90]	1st	1st
[45, −45, 90, 0]	2nd	3rd
[0, 90, −45, 45]	3rd	4th
[90, 0, −45, 45]	4th	2nd

Note: The buckling strength descending from top to bottom.

Table 6
Comparison between analytical and FEA solutions.

	Analytical	FEA	Deviation (%)
Specimen			
Buckling torque (Nm)	59.12	54.22	8.28
Natural frequency (Hz)	375.27	377.33	0.55
Drive shaft			
Buckling torque (Nm)	2030	1830.9	9.81
Natural frequency (Hz)	91.17	90.46	0.78

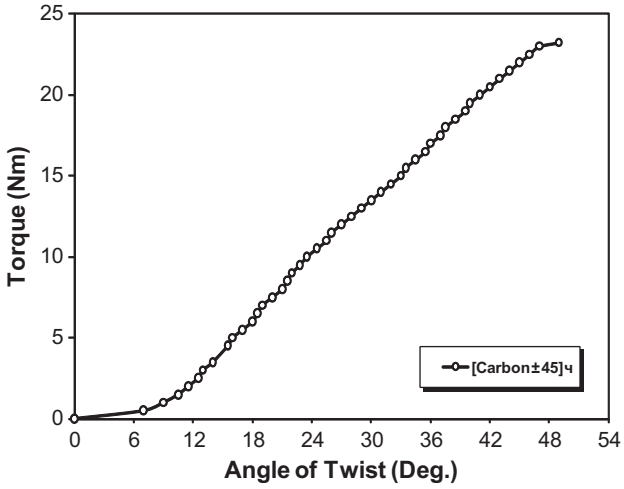

Fig. 21. Torque–angle of twist diagram for fabric fibers-composite in form of [carbon ±45]$_4$.

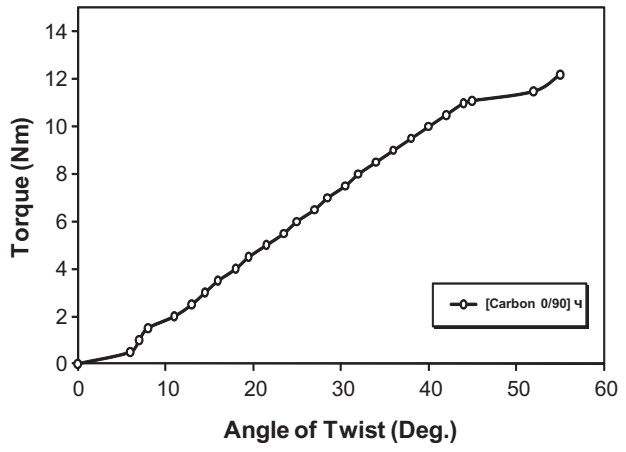

Fig. 20. Torque–angle of twist diagram for fabric fibers-composite in form of [carbon 0/90]$_4$.

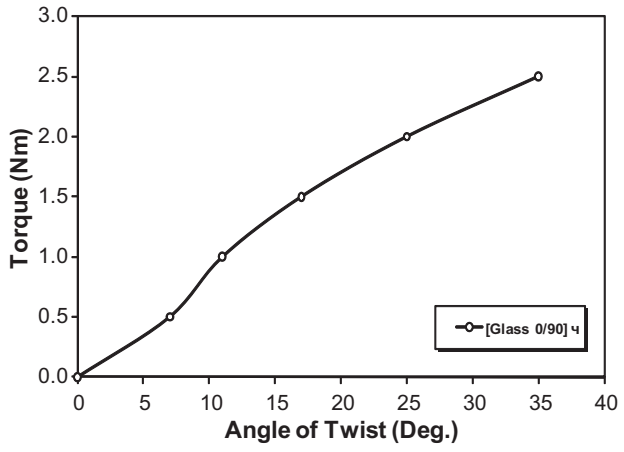

Fig. 22. Torque–angle of twist diagram for fabric fibers-composite in form of [glass 0/90]$_4$.

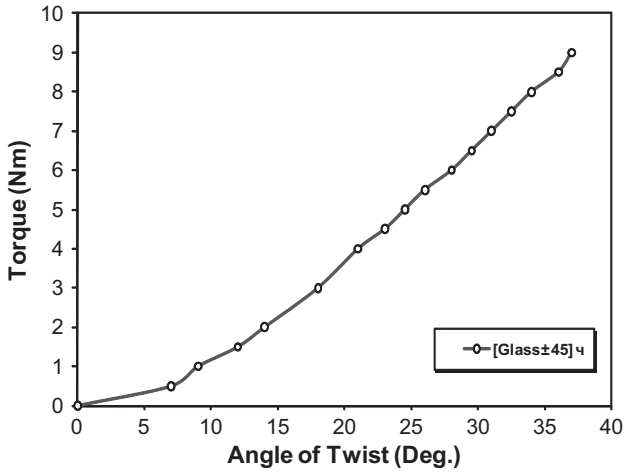

Fig. 23. Torque–angle of twist diagram for fabric fibers-composite in form of [glass ±45]$_4$.

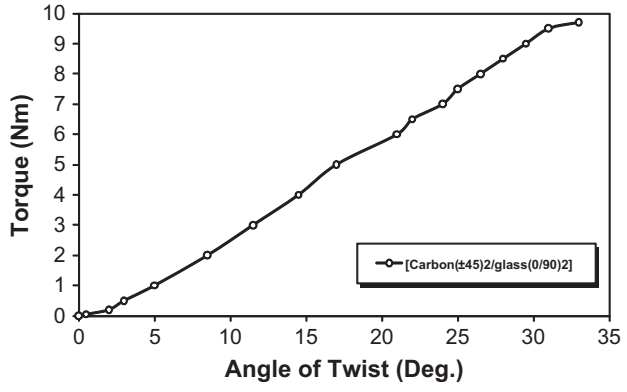

Fig. 24. Torque–angle of twist diagram for fabric fibers-composite in form of [carbon (±45)$_2$/glass (0/90)$_2$].

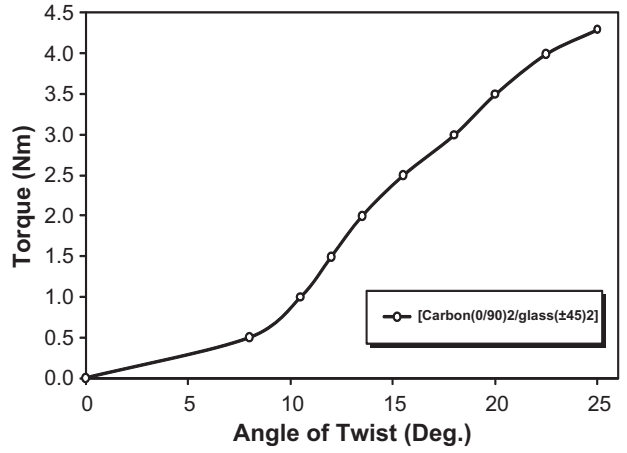

Fig. 25. Torque–angle of twist diagram for fabric fibers-composite in form of carbon (0/90)$_2$/glass (±45)$_2$].

have the same magnitude. Ranking of both fatigue and buckling strengths for different stacking sequences is presented in Table 5. Due to this ranking, the stacking configuration of [±45, 0, 90] fulfills both the best fatigue and buckling resistance characteristics because it satisfy the requirements of locating ±45 layers together and inside, in addition to locating 0/90 layers together with the 90° glass fibers orientation layer exposed to outside.

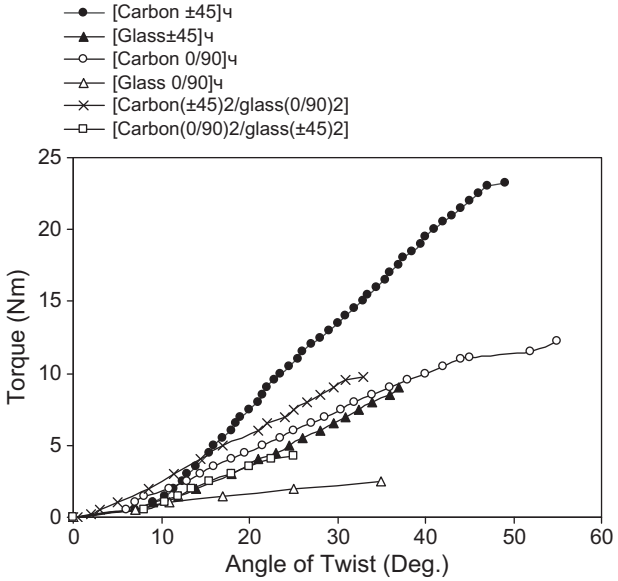

Fig. 26. Torsion response comparisons between six composite tubes.

6.1.6. Effect of physical dimensions on the failure mode

From the analysis of the full-scale drive shaft and one of the scaled down specimens used in the experimental work, it is clear that the dominant failure mode in the full-scale drive shaft is the buckling mode, while it is a shearing crack in the specimens as it could be shown from the experimental work. The same material as glass fabric/epoxy, the same fiber orientation angles (±45°) and the same number of plies were used in both the full-scale drive shaft and the specimen to define, analytically, their torques at which they buckle and the torques at which the fail under shearing cracks. The governing expressions for both types of torque are:

$$T_s = (2\pi r^2 t)\tau_{xy} \tag{11}$$

This expression gives the torque at which the composite tubes fail in a shearing crack mode and the following expression:

$$T_{cr} = (2\pi r^2 t)(0.272)[E_x E_h^3]^{0.25}(t/r)^{1.5} \tag{12}$$

The above equation defines the torque at which the composite tubes fail in buckling mode. The shearing torque for the full-scale drive shaft was 69.5 times that of the specimen. In addition, the buckling torque of the drive shaft is 23.6 times that of the specimen. This means that the strength of the drive shaft, with its current dimension, to resist failure under shear cracking is almost three times its strength to resist failure under buckling mode or that the failure is dominated by buckling in drive shaft and, in contrast, the (smaller radius) tubes fail by shear cracking. In this case, only the length of the radius is the factor in specifying the failure mode and in equalizing the two expressions we could obtain the radius that realize the occurrence of the two failure modes at the same torque. This is, indeed, a good concept to adjust the dimension in intension to allow the two failure modes occur at the same torque, but in the design optimization the radius is needed to be as longer as possible. In Table 6 a comparison between the analytical and FEA results is presented.

6.2. Experimental results

The experimental results for scaled down models of composite drive shaft under torsional loads will be presented and discussed. The failure critical torque and the correspondent angle of twist are measured to study the torsional stiffness and to investigate the devi-

Table 7
Comparison between torsional stiffness for six stacking sequence.

Stacking sequence	Torque (Nm)	Angle of twist (°)	Torsional stiffness (Nm/°)
All carbon $[\pm45^\circ]_4$	23.0	47	0.489
All carbon $[0/90]_4$	11.1	45	0.247
All glass $[\pm45^\circ]_4$	9.0	37	0.243
All glass $[0/90]_4$	2.5	35	0.071
Hybrid $[(\pm45)_2$carbon$/(0/90)_2$glass$]$	9.5	31	0.306
Hybrid $[(0/90)_2$carbon$/(\pm45)_2$glass$]$	4.0	22.5	0.178

ation of Finite Element Analysis results from the experimental ones. Eighteen specimens were fabricated to study the torsional stiffness of each one. Woven-roven fabrics of both carbon and glass fibers were impregnated with epoxy to make laminates of four layers. These layers stacked at two fiber orientation angles as ±45 and 0/90, which can referred to as 45 and 90. Beside, a hybrid of both carbon/epoxy and glass/epoxy was used. The static torsion test for the previous six structures was carried out by applying the torque manually and gradually. The results of this test indicate the rigidities of different composite structures utilizing different materials and fibers orientation angles. The torsional stiffness is directly related to the modulus of rigidity. It is clear from Figs. 20–26 that, the static failure torque of 45° fibers orientation is higher than 90°. According to the classical lamination theory, the in-plane shear stiffness component A_{66} is larger for any laminate having the structure of $[\pm45]_n$ than laminate having the structure of $[90/0]_n$, therefore the specimens with 45° layers sustain higher loads with less corresponding shear strain. On the other hand, carbon fibers show higher torque carrying capability than glass fibers. The low slopes in Figs. 19–21 and 25 initial curves are due to nonperforming of a "shake-down" process on the specimen's set-up. It can be observed that the failure of ±45° stacking in both carbon and glass laminates occurs suddenly while the stacking of 90/0 experienced gradual failure. This phenomenon attributed to that, the fibers at ±45 bear the maximum shear stress until this stress reaches the shear strength of the material and catastrophic failure takes place. In the case of 90/0 stacking the fibers at 0° bear the in-plane shear stress and the fibers at 90°, in the same layer, bear a less magnitude of the associated shear stress developed along an axial plane. Indeed, it is the same as in buckling strength presented previously; the fibers at 90° withstand higher stress than at 0°. For this reason the failure occurs first at fibers oriented at 0° angle and the mode is a crack along the hoop direction. From Figs. 25 and 26, the use of hybrid tubes realizes the occurrence of an intensive matrix cracks at the outer plies. These matrix cracks extended in the case of the configuration of less stiffness difference [carbon $(0/90)_2$/glass $(\pm45)_2$]. It is proven that the use of materials of different stiffness in the load carrying ply of a laminate to contain crack movement. Fig. 26 presents a comparison between the torsion responses of the six specimens. It is clear that the carbon-epoxy specimens experience smaller angles of twist than the glass–epoxy specimens for the same value of torque because the ratio of torque to angle of twist, which is proportional to the shear modulus, keep constant until the failure torque applied. It is perceived that both carbon and glass fibers are almost completely brittle, hence only the fibers architecture specify the ductile-like-behavior. The hybrid of carbon and glass–epoxy with the stacking of [carbon $(\pm45)_2$/glass $(0/90)_2$] shows initially suppressed angle of twist. This strain retaining is higher than that of the all carbon ±45 specimens at the first stage of applying the load. This phenomena could be attributed to the load path locking as this load transferred between layers having severe difference in stiffness like the difference between ±45° carbon layers and 0/90 glass layers. Also from the shape of the plot for the hybridized specimens, it is recognized that the carbon layers are dominant in the torque–angle of twist behavior. From Fig. 26, there are four configurations have the same torsional stiffness. These configurations are the two hybrids, [glass $\pm45]_4$ and [carbon $0/90]_4$. It is obvious in comparing these configurations that carbon fibers torque tubes experience higher fracture strain than that fabricated from glass fibers despite the higher elongation percent of E-glass/epoxy (2.5%) in comparison with the elongation of high modulus carbon/epoxy (0.6%). The higher fracture strain of the carbon/epoxy torque tubes is attributed to the nature of carbon fibers that have a very low transverse modulus, which is equal to about 3–10% of the axial modulus. In contrast, the properties of glass fibers are isotropic. The carbon fibers with their low transverse modulus and hence higher flexibility to torque loading provide the property of higher fracture toughness for the composite tubes utilizing them. From Table 7, it is clear that the torsional stiffness not only related to the type of fibers used but also to the fiber orientation angle. The torsional spring rate (i.e. the torsional stiffness) can be tailored in composites. In this experiment the torsional spring rate of all carbon $[\pm45]_4$ stacking is 6.9 times that of all glass $[0/90]_4$ stacking.

6.2.1. Failure modes

Three distinct failure modes were observed and presented in Fig. 27. These modes has been identified and classified as follows.

6.2.1.1. Catastrophic failure. Catastrophic failure, in which the inter-fiber failure is the dominant mode of failure. Failure initiation was characterized by fiber fractures, splitting of the laminates parallel to fibers and some debonding between adjacent layers of the laminates. The growth of damage at the 45° fiber/matrix interface causes a weakened area where failure is initiated. This type of mode is associated to tubes with $[\pm45^\circ]_4$ lay-up.

6.2.1.2. Progressive failure mode. In this failure mode, the growth of damage is observed to be at either 90° or 45° fiber/matrix interface causes a weakened area where failure is initiated. The fracture direction is observed to be material dependent. Fracture growth

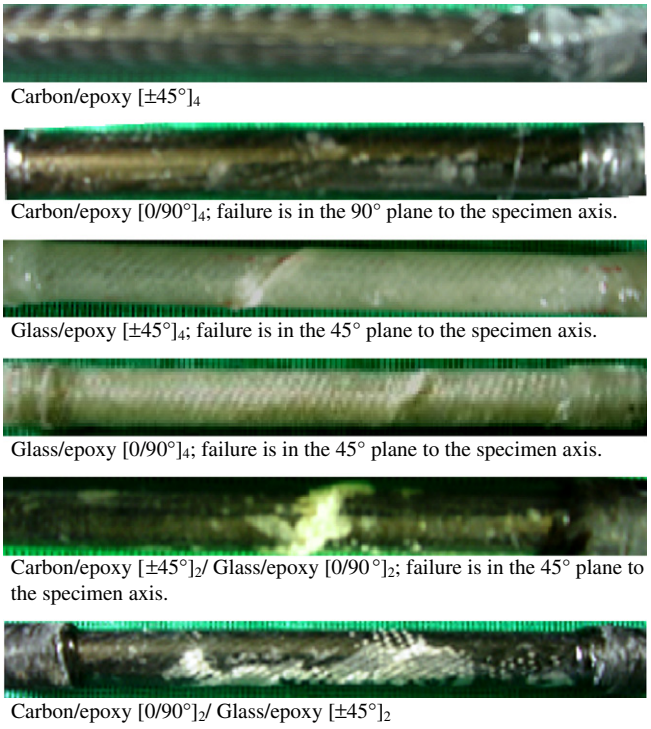

Fig. 27. Failure modes for hybrid and non-hybrid composite tubes subjected to pure torsion.

at 90° is exhibited by carbon tubes, while fracture growth at 45° is associated to glass tubes. This failure is associated to tubes with $[0/90°]_4$ lay-up. Since the matrix material (epoxy) is not very weak compared to the fiber (E_m = 3.4 GPa), so the matrix and the 90° oriented fiber prevent the 0° oriented fiber from local micro-buckling under small load. For the fiber oriented at 90° where the load is directed parallel, most probably failure will be initiated at stress level corresponds to the shear of the matrix. No stiffness reduction is considered due to matrix failure. This is because transverse matrix cracks alone usually do not have significant effect on the laminate stiffness. The matrix crack leads to debonding, which results in local surface ply separation (local delamination) and fiber breakage.

6.2.1.3. Mix failure mode. This failure mode is associated to hybrid composite tubes subjected to pure torsional load. It is observed that [±45°] configuration influenced the failure mode. There are a number of locations where final failure of the composite may initiate. However, it was observed during the experiment that final failure initiated in the outer layer at 45° to the specimen axis. After fiber/matrix debonding occurred, the local stress field becomes very complex and the normal and shear stresses caused delamination of subsequent layers.

7. Conclusion

From the previously presented results, the following conclusion can be drawn as follows:

7.1. Effects on natural frequency

- The bending natural frequency increase by decreasing the fiber orientation angle. Decreasing the angle increase the modulus in the axial direction.
- The decrease of fiber orientation angle to increase the natural frequency is not monotonic; with thickness equal to almost 0.14 of the drive shaft thickness, the frequency higher value is at 38° angle, at which the torque coupling coefficient has its maximum value and hence a higher membrane stiffness augments the bending stiffness of the composite tube and increasing the natural frequency.
- The layers stacking sequence has no effect on the natural frequency since there is no load applied.
- The component D_{16} corresponds to coupling between twist moment and normal curvature at axial direction has an effect on the natural frequency in applying loads to the drive shaft. As the load increases, the natural frequency decreases.
- The predicted natural frequency agrees with analytical solution with a deviation of 0.78%.

7.2. Effects on buckling torque

- Fibers orientation angle has an effect on the buckling torque.
- To increase the buckling torque, the modulus at hoop direction must be increased by orienting fibers to approach a 90° angle.
- Changing the fiber orientation angle of one or more layer may not gives a proportionality of buckling torque to the increase of angles. This is related to the effect of the modulus along the axial direction (E_x) and the modulus at the hoop direction (E_h) as the former has its maximum value at 0° angle and the later at 90° angle. Result can be as best at 90°, good at 0° and worst at 40° angles.
- Stacking sequence has a big effect on the buckling torque.
- The measuring factor of the buckling torque is a component in the bending stiffness matrix [D]. This component is the normal bending stiffness along the hoop direction [D_{22}], and it specifies the resistance of the drive shaft to deflect radially toward inside or (buckled).
- The component D_{26} corresponds to coupling between twist moment and normal curvature at hoop direction has an effect on the buckling strength and the sign of this component specify whether the cross-section diameter increases or decreases. With another word, specify resisting or supporting the buckling of the torque tube.
- From 15 different stacking sequences analyzed in this study, the worst stacking realize a loss of 46.07% of the critical buckling torque when the best stacking applied.
- The FEA prediction of buckling torque deviate by 9.81% from that resulted from analytical solution.

7.3. Effects on fatigue life

- The stacking sequence has an effect on the fatigue resistance.
- The best stacking is to locate the layers of ±45° fiber orientation angles together and far near the inner face of the torque tube. In addition, the cross-ply configuration must be located exposed to outside with the seniority of the 90° layer at the outer face location.
- The gripped zones at both ends of the drive shaft sustain higher degrees of damage turned over to be of a shorter life.

7.4. Torsional stiffness and failure modes

- Carbon fibers have the major contribution over glass in increasing the torsional stiffness.
- The fiber orientation angle of 45° is the best in increasing the torsional stiffness.
- Laminates containing fabric fibers placed at ±45° experienced sudden failure whatever the material is. On the other hand, the stacking of 90/0 experienced a progressive and gradual failure.
- Carbon/epoxy tubes experience higher fracture strain than that of glass/epoxy.
- In hybridized tubes, the severe difference in torsional stiffness of the layers leads to initially suppressed twisting.
- In hybridized tubes, the severe difference in torsional stiffness of the layers leads to contain the matrix cracks at outer plies not to extend towards the tubes ends.
- In a hybrid of carbon fabric and glass fabric composites, the failure mode was dominated by [±45°] configuration.

8. Recommendations for further work

Suggestions for further work are listed as follows:

- Effect of joints geometry on the bending natural frequency
- Utilization of pre-pregnated, pre-tensioned 45° threaded fibers winding for power transmission tubes.
- Effect of adhesive bonding of short ±45° fabric composite tubes at inner surface on damage tolerance and natural frequency.
- As the dominant failure mode in drive shafts is buckling, a study can be carried out to investigate the effect of composite ring stiffener on the buckling torque and natural frequency. This study can be extended to find the optimum locations along the shaft span i.e. two stiffeners located at 40% and 60% of the axial distance because buckling not initiated at the centre and dynamic balance considered.

References

[1] McGeehi P. Composites in transportation: design and current developments. Mater Des 1982;3(2):378–87 [available online 2003].

[2] Khalid YA, Mutasher SA, Sahari BB, Hamouda AMS. Bending fatigue behavior of hybrid aluminum/composite drive shafts. Mater Des 2007;28(1):329–34.
[3] Leslie JC, Troung L, Blank B, Frick G. Composite driveshaft: technology and experience. SAE Special Publications 1996;1203:43–52.
[4] Mutasher SA. Prediction of the torsional strength of the hybrid aluminum/composite drive shaft. Mater Des 2009;30(2):215–20.
[5] Rastogi N. Design of composite driveshafts for automotive applications. SAE, technical paper series, 2004-01-0485; 2004.
[6] Shokrieh Mahmood M, Hasani Akbar, Lessard Larry B. Shear buckling of a composite drive shaft under torsion. Compos Struct 2004;64:63–9.
[7] Topal Umat. Multi objective optimization of laminated composite cylindrical shells for maximum frequency and buckling load. Mater Des 2009;30(7):2584–94.
[8] Silvestre N. Generalized beam theory to analyze the buckling behavior of circular cylindrical shells and tubes. Thin-Walled Struct 2007;45(2):185–98.
[9] Bert CW, Kim CD. Analysis of buckling hollow laminated composite drive shafts. Compos Sci Technol 1995;53:343–51.
[10] Chen LW, Kung Peng W. The stability behavior of rotating composite shafts under axial compressive loads. Compos Struct 1998;41:253–63.
[11] Cook RD, Malkus DS, Plesha ME, Witt RJ. Concepts and applications of finite element analysis. 4th ed. New York: John Wiley & Sons; 2002.
[12] Mitrovic M, Hahn HT, Carman GP, Shyprykevich P. Effect of loading parameters on the fatigue behavior of impact damaged composite laminates. Compos Sci Technol 1999;59(14):2059–78.
[13] Wang Shi-Xun, Wu Lin-Zhi, Ma Li. Low-velocity impact and residual tensile strength analysis to carbon fiber composite laminates. Mater Des 2010;31(1):118–25.
[14] Zhang Yan, Zhu Ping, Lai Xinmin. Finite element analysis of low-velocity impact damage in composite laminated plates. Mater Des 2006;27(6):513–9.
[15] Aymerich F, Priolo P. Characterization of fracture modes in stitched and unstitched cross-ply laminates subjected to low-velocity impact and compression after impact loading. Int J Impact Eng 2008;35(7):591–608.
[16] Cho DH, Lee DG. Manufacture of one-piece automotive drive shafts with aluminum and composite materials. J Compos Struct 1997;38(1–4):309–19.
[17] Herakovich CT. Influence of layer thickness on the strength of angle-ply laminates. J. Compos. Mater 1982;16:216.
[18] LUSAS, User's manual, version 13.7-5.
[19] Jones RM. Mechanics of composite materials. 2nd ed. Philadelphia: Tailor Francis; 1999.
[20] Swanson SR. Introduction to design and analysis with advanced composite materials. Upper Saddle River, New Jersey: Prentice Hall; 1997.